THE JOURNAL OF BIOLOGICAL CHEMISTRY VOL. 286, NO. 31, pp. 27515–27527, August 5, 2011

Arabidopsis Chloroplastic Glutaredoxin C5 as a Model to Explore Molecular Determinants for Iron-Sulfur Cluster Binding into Glutaredoxins*[S]

Received for publication, February 7, 2011, and in revised form, May 17, 2011 Published, JBC Papers in Press, June 1, 2011, DOI 10.1074/jbc.M111.228726

Jérémy Couturier[‡§1], Elke Ströher[§1], Angela-Nadia Albetel[¶1], Thomas Roret[‖1], Meenakumari Muthuramalingam[§], Lionel Tarrago[‡], Thorsten Seidel[§], Pascale Tsan[‖], Jean-Pierre Jacquot[‡], Michael K. Johnson[¶], Karl-Josef Dietz[§], Claude Didierjean[‖2], and Nicolas Rouhier[‡3]

From the [‡]Unité Mixte de Recherches (UMR) 1136, Institut National de la Recherche Agronomique-Nancy Université, Interactions Arbres Microorganismes, Institut Fédératif de Recherche 110 Ecosystèmes Forestiers, Agroressources, Biomolécule et Alimentation, 54506 Vandoeuvre-lès-Nancy Cedex, France, [§]Faculty of Biology-W5-134, University of Bielefeld, D-33501 Bielefeld, Germany, [¶]Department of Chemistry and Center for Metalloenzyme Studies, University of Georgia, Athens, Georgia 30602, and [‖]Cristallographie, Résonance Magnétique et Modélisations, Equipe Biocristallographie, UMR 7036 CNRS-Université Henri Poincaré Faculté des Sciences et Technologies, Nancy Université, BP 239, 54506 Vandoeuvre-lès-Nancy Cedex, France

Unlike thioredoxins, glutaredoxins are involved in iron-sulfur cluster assembly and in reduction of specific disulfides (*i.e.* protein-glutathione adducts), and thus they are also important redox regulators of chloroplast metabolism. Using GFP fusion, AtGrxC5 isoform, present exclusively in Brassicaceae, was shown to be localized in chloroplasts. A comparison of the biochemical, structural, and spectroscopic properties of *Arabidopsis* GrxC5 (WCSYC active site) with poplar GrxS12 (WCSYS active site), a chloroplastic paralog, indicated that, contrary to the solely apomonomeric GrxS12 isoform, AtGrxC5 exists as two forms when expressed in *Escherichia coli*. The monomeric apoprotein possesses deglutathionylation activity mediating the recycling of plastidial methionine sulfoxide reductase B1 and peroxiredoxin IIE, whereas the dimeric holoprotein incorporates a [2Fe-2S] cluster. Site-directed mutagenesis experiments and resolution of the x-ray crystal structure of AtGrxC5 in its holoform revealed that, although not involved in its ligation, the presence of the second active site cysteine (Cys^{32}) is required for cluster formation. In addition, thiol titrations, fluorescence measurements, and mass spectrometry analyses showed that, despite the presence of a dithiol active site, AtGrxC5 does not form any inter- or intramolecular disulfide bond and that its activity exclusively relies on a monothiol mechanism.

Glutaredoxins (Grxs)[4] are thiol-disulfide oxidoreductases present in most prokaryotic and eukaryotic organisms and belonging to the thioredoxin (Trx) superfamily (1, 2). At the structural level, proteins of the Trx superfamily share the so-called Trx fold, which consists of four-stranded β-sheets surrounded by at least three α-helices (3). Using a C*XX*C or C*XX*S active site motif, Grxs are involved in the reduction of glutathionylated proteins. The regeneration of an active reduced form usually relies on glutathione (GSH), but some specific members such as human Grx2, *Escherichia coli* Grx4, and *Chlamydomonas reinhardtii* Grx3 are also or uniquely regenerated by thioredoxin reductases (4–6). This variation correlates with the type of Grx considered and depends on their redox potential and catalytic mechanism. Indeed, whereas classical Grxs have midpoint redox potentials between −170 and −230 mV (pH 7.0) (7, 8), *Chlamydomonas* Grx3 forms during its catalytic cycle an atypical intramolecular disulfide between the first active site cysteine and a second cysteine located in the C-terminal part of the protein (6). The more negative redox potential (−323 mV at pH 7.9) observed for this protein most likely explains its ability to receive electrons from ferredoxin:thioredoxin reductase but not from glutathione (6).

The initial Grx classification in non-plant organisms was first based on the active site sequences and resulted in defining two Grx types containing either a dithiol (CP(Y/F)C) or a monothiol (usually CGFS) active site motif (9). However, with the identification of new Grx sequences with more variable active site sequences, this classification has become insufficient. In particular, photosynthetic organisms possess a larger variety of Grxs with about 30 genes compared with two to seven in other prokaryotes or eukaryotes (10). An in-depth phylogenetic analysis of Grxs in photosynthetic organisms indicates that they are grouped into four classes (11). Class I includes "classical" Grxs with CPYC, CGYC, CPFC, or CSY(C/S) active sites and is sub-

* This work was supported, in whole or in part, by National Institutes of Health Grant GM62524 (to M. K. J.). This work was also supported by the Alexander von Humboldt Foundation (to J. P. J.), Agence Nationale de la Recherche Grant JC07_204825 (to J. C. and N. R.), and Deutsche Forschungsgemeinschaft Grant Di346-14 (to K. J. D.).

[S] The on-line version of this article (available at http://www.jbc.org) contains supplemental Tables 1–3 and Figs. 1–4.

The atomic coordinates and structure factors (codes 3RHB and 3RHC) have been deposited in the Protein Data Bank, Research Collaboratory for Structural Bioinformatics, Rutgers University, New Brunswick, NJ (http://www.rcsb.org/).

[1] These authors contributed equally to this work.

[2] To whom correspondence may be addressed. Tel.: 33383684879; E-mail: Claude.Didierjean@crm2.uhp-nancy.fr.

[3] To whom correspondence may be addressed. Tel.: 33383684225; E-mail: nrouhier@scbiol.uhp-nancy.fr.

[4] The abbreviations used are: Grx, glutaredoxin; GSH, reduced glutathione; Trx, thioredoxin; At, *A. thaliana*; Pt, poplar; HED, 2-hydroxyethyl disulfide; CFP, cyan fluorescent protein; DTT_{red}, reduced DTT; DTT_{ox}, oxidized DTT; GSSG, oxidized glutathione; DHA, dehydroascorbate; Prx, peroxiredoxin; Cr, *C. reinhardtii*.

divided into five subgroups called GrxC1, -C2, -C3, -C4 and -C5/S12. Class II contains Grxs with a conserved CGFS active site and is divided into four subgroups called GrxS14, -S15, -S16, and -S17. In addition, class III, which contains Grxs with a *CCXX* active site motif, is found in terrestrial plants, and class IV, which consists of multidomain proteins containing in their N-terminal part a Grx module, is present in eukaryotic photosynthetic organisms (11).

Through their disulfide reductase activity, class I Grxs are involved in the stress response, catalyzing the reduction of dehydroascorbate (12), and the regeneration of type II peroxiredoxins (13) and 1-Cys methionine sulfoxide reductase B1 (14, 15). These regeneration mechanisms likely occur via a glutathionylation step. Although Trxs have been reported to catalyze deglutathionylation in some organisms (16), this reaction is generally considered to be specifically catalyzed by Grxs (17). Protein deglutathionylation can proceed via a monothiol or a dithiol pathway depending on the involvement of one or two cysteines in the catalytic mechanism (6, 18, 19).

Besides its disulfide reductase activity, a novel function assigned to some bacterial, yeast, human, and plant class II Grxs is their involvement in the iron-sulfur (Fe-S) cluster assembly machinery most likely through their capacity to incorporate labile Fe-S clusters and transfer them to acceptor proteins (20–22). On the other hand, specific class I Grxs such as human Grx2 and plant GrxC1 also have the capacity to incorporate Fe-S clusters that are more stable than those found in class II Grxs (8, 23). Based on the observation that oxidized glutathione promotes cluster disassembly in human Grx2, it has been hypothesized that under defined redox conditions the release of Grxs in an active form might serve as a redox sensor in human cells (23).

The determination of the three-dimensional structure of poplar GrxC1 and human Grx2 indicated that the [2Fe-2S] cluster was ligated into a homodimer by the N-terminal active site cysteine of two monomers and two glutathione molecules (8, 24, 25). A similar ligation was observed for *E. coli* Grx4, a class II Grx, but the different orientation of the two monomers was proposed to be responsible for the differential cluster lability (26). The capacity of class I Grxs to bind an Fe-S cluster has been studied in detail by site-directed mutagenesis, and it was proposed that the nature of the residues adjacent to the first active site Cys determined this capacity (8, 27). In particular, for Grxs with a YCPFC or YCPYC active site, the replacement of the proline by a glycine, simulating GrxC1 (YCGYC), was sufficient to allow the incorporation of such a cluster (8) In addition, it has been hypothesized that the Trp residue adjacent to the catalytic cysteine residue in GrxS12 (WCSYS active site) prevented cluster incorporation because changing it into a Tyr allowed cluster incorporation (27).

A close paralog of GrxS12 having a WCSYC active site and named GrxC5 is present only in Brassicaceae. Here we have investigated the structure-function relationship of *Arabidopsis thaliana* GrxC5 (AtGrxC5) and compared it to poplar GrxS12 (PtGrxS12). The putative role of this Grx in plastids of Brassicaceae is discussed in the light of other functions identified so far for other Grx members.

EXPERIMENTAL PROCEDURES

Materials—G25 columns were purchased from GE Healthcare. 2-Hydroxyethyl disulfide (HED) and 5,5′-dithiobis-2-nitrobenzoic acid were from Acros Organics and Pierce, respectively. All other reagents were from Sigma.

Cloning and Construction of AtGrxC5 and PtGrxS12 Mutants by Site-directed Mutagenesis—The open reading frame sequence encoding *A. thaliana* GrxC5 (At4g28730) was amplified from leaf cDNA using AtGrxC5 forward and reverse primers (supplemental Table 1) and cloned into pET3d. The amplified sequence encodes a protein deprived of the first 63 amino acids corresponding to the putative targeting sequence and in which a methionine and an alanine have been added during cloning. The protein thus starts with the N-terminal sequence ^{1}MASFGSRM^{8} and ends with ^{98}GKNGQS^{113} at the C terminus. Using two complementary mutagenic primers, the four cysteines of AtGrxC5 were individually substituted into serines. The mutated proteins are called AtGrxC5 C29S, C32S, C80S, and C87S. Various combinations of cysteine substitutions by serine were also introduced in GrxC5 (C29S/C32S and C80S/C87S). In addition, to mimic the active site of AtGrxC5, a PtGrxS12 S32C variant was produced with the serine in position 32 modified into a cysteine. The primers are listed in supplemental Table 1.

Expression and Purification of Recombinant Proteins—For protein production, the *E. coli* BL21(DE3) strain, containing the pSBET plasmid, was co-transformed with the different recombinant plasmids (28). Cultures were successively amplified up to 2.4 liters in LB medium supplemented with ampicillin and kanamycin (50 $\mu g \cdot ml^{-1}$) at 37 °C. Protein expression was induced at exponential phase by adding 100 μM isopropyl β-D-thiogalactopyranoside for 4 h at 37 °C. The cultures were then centrifuged for 15 min at 4,400 × *g*. The pellets were resuspended in 30 ml of Tris-NaCl (30 mM Tris-HCl, pH 8.0, 200 mM NaCl) buffer with 1 mM GSH, and the cells were stored at −20 °C.

Cell lysis was performed by sonication (3 × 1 min with intervals of 1 min), and the soluble and insoluble fractions were separated by centrifugation for 30 min at 27,000 × *g*. The soluble part was then fractionated with ammonium sulfate in two steps, and the protein fraction precipitating between 40 and 80% saturation contained the recombinant protein as estimated by 15% SDS-PAGE. AtGrxC5 WT, C80S, and C87S and poplar GrxS12 S32C were purified by size exclusion chromatography after loading on an ACA44 (5 × 75-cm) column equilibrated in Tris-NaCl buffer usually supplemented with 100 μM GSH. However, some purifications were achieved without GSH. The fractions containing the protein were pooled, dialyzed by ultrafiltration to remove NaCl, and loaded onto a DEAE (diethylaminoethyl)-cellulose column (Sigma) equilibrated in a 30 mM Tris-HCl pH 8.0 buffer. The recombinant proteins passed through the DEAE column, were concentrated by ultrafiltration under nitrogen pressure (Amicon, YM10 membrane), and were stored in the same buffer at −20 °C.

Because they were mainly insoluble in the above described culture conditions, the culture and purification conditions of AtGrxC5 C29S and C32S were slightly modified following a

procedure described previously (29). Protein purity was checked by SDS-PAGE, and protein concentrations were determined spectrophotometrically using a molar extinction coefficient at 280 nm of 8,730 M^{-1} cm^{-1} for AtGrxC5 WT; 8,605 M^{-1} cm^{-1} for AtGrxC5 C29S, C32S, C80S, C87S, C29S/C32S, and C80S/C87S; and 10,095 M^{-1} cm^{-1} for PtGrxS12 S32C. PtGrxC1, PtGrxC3, PtGrxS12, PtTrxh1, AtMsrB1, and AtPrxIIE were purified as described previously (8, 14, 27, 30, 31).

Transcript Analysis—Four to 5-week-old plants were used for the analysis of transcript levels of the four plastidial Grxs (GrxC5, -S12, -S14, and -S16). *A. thaliana* ecotype Columbia was grown on soil under controlled conditions (10 h of light at 100 μmol quanta m^{-2} s^{-1} and 23 °C and 14 h of darkness at 18 °C; 50% relative humidity). Four hours after the onset of light, selected stress treatments were started. Cold stress was performed at 4 °C, and salt stress was applied by extensively watering the pots with 200 ml of 150 and 300 mM NaCl solution, respectively. A similar osmotic treatment was performed with 15% (w/v) PEG-5000 (same osmolarity as 150 mM NaCl). Complete rosettes of control and treated plants were harvested after 24 h, frozen immediately in liquid nitrogen, and stored at −80 °C. RNA isolation and the subsequent cDNA synthesis were performed according to Wormuth *et al.* (32). Supplemental Table 1 lists the combinations of primers used.

In Vivo Subcellular Localization by GFP Fusions—The putative targeting sequences of AtGrxC5, AtGrxC10 (At5g11930), AtGrxS12 (At2g20270), AtGrxS13 (At1g03850), AtGrxS14 (At3g54900), and AtGrxS16 (At2g38270) were cloned into the 35S-CFP-NosT or 35S-YFP-NosT vector between BamHI and AgeI restriction sites using primer combinations described in supplemental Table 1. The isolation, transfection of *A. thaliana* mesophyll protoplasts, and final fluorescence microscopy of protoplasts were performed according to Seidel *et al.* (33).

Electrospray Ionization-MS Analysis of Reduced and Oxidized Proteins—Three to 5 mg of proteins were reduced using 20 mM DTT_{red} for 15 min at 25 °C followed by desalting on G25 columns pre-equilibrated with 30 mM Tris-HCl, pH 8.0, 1 mM EDTA (TE) buffer. Oxidized Grxs were prepared by incubating prereduced Grxs with either 1 mM GSSG or 20 mM DTT_{ox} for a 15-min or longer period at 25 °C before desalting on G25 columns.

High resolution electrospray ionization-MS spectra of treated and untreated proteins were obtained on a Bruker microTOF-Q spectrometer (Bruker Daltonics, Bremen, Germany) equipped with an Apollo II electrospray ionization source with an ion funnel and operated in the negative ion mode. A concentrated sample (around 100 μl at 100 μM) in formic acid was injected at a flow rate of 10–20 μl min^{-1}. The potential between the spray needle and the orifice was set to 4.5 kV. Before each run, the instrument was calibrated externally with the Tunemix™ mixture (Agilent Technologies) in quadratic regression mode. Data were analyzed with DataAnalysis software (Bruker).

Fluorescence Properties of AtGrxC5—The intrinsic fluorescence of AtGrxC5 WT and mutants in the reduced and oxidized forms was recorded with a Cary Eclipse spectrofluorometer (Varian) with 10 μM samples in TE buffer and an excitation wavelength fixed at 270 nm. Control spectra were run with buffer only for each sample and subtracted from the spectra.

Thioltransferase Activity (HED and Dehydroascorbate (DHA) Assays)—The HED reduction was measured at 25 °C in steady-state conditions by following NADPH oxidation at 340 nm in the presence of a Grx reducing system. A 500-μl reaction mixture in 30 mM Tris-HCl, pH 8.0, 1 mM EDTA buffer contained 150 μM NADPH, 0.5 units of glutathione reductase from bakers' yeast, 2 mM GSH, 0.7 mM HED, and 400 nM Grx except for AtGrxC5 C32S (200 nM Grx). The dehydroascorbate reductase activity was measured using a similar method except that the test was performed in 100 mM phosphate pH 7.0 buffer with 1 mM DHA and 2 μM Grx (1 μM for AtGrxC5 C32S). The reaction was started by adding Grx after a 2-min preincubation. Grx activity was determined by subtracting the spontaneous reduction rate observed in the absence of Grx. The activity was expressed as nmol of NADPH oxidized/nmol of Grx/min using a molar extinction coefficient of 6,220 M^{-1} cm^{-1} at 340 nm for NADPH. Three independent experiments were performed at each substrate concentration, and the apparent k_{cat} and K_m values were calculated by non-linear regression using the program GraphPad Prism 4.

Insulin Reduction—Insulin reduction was monitored spectrophotometrically at 30 °C using 2 μM Trx or 10 μM Grx and a procedure described previously (29).

Glutaredoxin-dependent Peroxidase Activity of PrxIIE—Rates of peroxide reduction by PrxIIE were determined in an assay coupled with the glutaredoxin system by monitoring NADPH oxidation following absorbance at 340 nm. The assay typically contained 50 μM *t*-butyl hydroperoxide in 100 mM HEPES pH 8.0 buffer, 2 mM EDTA, 1 mM GSH, 150 μM NADPH, 2 μM PrxIIE, and from 0.1 to 6 μM Grx. The comparative mutant analysis was then performed with 1 μM Grx.

Methionine Sulfoxide Reductase Activity Assay—The MsrB1 activity was measured by following NADPH oxidation at 340 nm in the presence of a Grx reducing system at 25 °C. A 500-μl reaction mixture in 30 mM Tris-HCl, pH 8.0, contained 200 μM NADPH, 0.5 units of glutathione reductase from bakers' yeast, 10 mM GSH, 2 mM *N*-acetylmethionine sulfoxide, 2.5 μM MsrB1, and 25 μM AtGrxC5 corresponding to a saturating concentration. MsrB1 activity was calculated as described previously (14).

Analytical and Spectroscopic Methods—Analytical gel filtration analyses were performed with an ÄKTA Avant system (GE Healthcare). 150 μl at about 100 μM apo- and holoforms were separately loaded on a Superdex 75 HR 10/30 column (GE Healthcare) equilibrated with 50 mM Tris-HCl, pH 8.0, 150 mM NaCl and calibrated with gel filtration standards (Bio-Rad). Elution profiles were simultaneously recorded at 280 and 430 nm with a flow rate of 0.5 ml min^{-1}.

Protein concentrations were determined by using BSA as a standard using the Bio-Rad DC protein assay in conjunction with the microscale modified procedure of Brown *et al.* (34). Iron concentrations were determined colorimetrically by using bathophenanthroline under reducing conditions after digestion of the protein in 0.8% $KMnO_4$, 0.2 M HCl (35). Fe-S cluster reconstitution experiments in AtGrxC5 C32S were carried out under anaerobic conditions following a procedure described

previously (20). UV-visible absorption and CD spectra were recorded at room temperature using a Shimadzu UV-3101PC spectrophotometer and Jasco J-715 spectropolarimeter, respectively. Resonance Raman spectra were recorded as described previously (36) using an Instruments SA Ramanor U1000 spectrometer coupled with a Coherent Sabre argon ion laser with 20-μl frozen droplets of sample mounted on the cold finger of an Air Products Displex Model CSA-202E closed cycle refrigerator.

Crystallization, Data Collection, Structure Determination, and Crystallographic Refinement—Crystallization experiments were performed by the microbatch under oil (paraffin) method at 4 °C under aerobic conditions. Drops were prepared by mixing 1.5 μl of protein solution with an equal volume of crystallization solution. Solutions of apo- and holoproteins had concentrations of 8.9 and 16.7 mg·ml^{-1}, respectively. Suitable crystals for x-ray diffraction were obtained without optimization using crystallization screen kits. The apoform crystallized in 1.6 M ammonium sulfate and 500 mM lithium chloride (Jena Biosciences, JBS 5-B4), whereas brownish crystals were obtained for the holoform by using 0.1 M HEPES, pH 7.5 and 70% 2-methyl-2,4-pentanediol solution (Hampton Research crystal screen 2-35). X-ray diffraction experiments were performed at 100 K with holoform crystals flash cooled directly from the drop and apoform crystals and soaked briefly in crystallization solution supplemented with 20% (v/v) glycerol. Apo- and holoform data sets were collected on beamlines BM30A and ID23–1 at the European Synchrotron Radiation Facility (Grenoble, France), respectively. The data were indexed and processed using XDS (37) and scaled and merged with SCALA from the CCP4 program package (38, 39). Both structures were solved by molecular replacement with MOLREP (40) using the poplar GrxS12 coordinates (Protein Data Bank code 3FZ9). The models were refined using REFMAC version 5.4 (41) interspersed with manual inspection and corrections using COOT (42). In the final rounds of apoform refinement, anisotropic B-factors were included for selected atoms. The validation of both crystal structures was performed with MOLPROBITY (43). All figures were prepared with PyMOL. All statistics are available in Table 1.

TABLE 1
Statistics of x-ray diffraction data collection and model refinement

	Apoform	Holoform
Data collection		
Space group	$P2_12_12$	$R3$
Cell dimensions *a*, *b*, *c* (Å)	63.5, 39.0, 37.6	111.7, 111.7, 58.5
Resolution (Å)	33.25-1.2 (1.26-1.20)[a]	27.99-2.4 (2.53-2.4)[a]
R_{merge}	0.052 (0.221)	0.061 (0.33)
Mean $I/\sigma(I)$	21.9 (4.9)	15.5 (5.2)
Completeness (%)	94 (68)	99 (100)
n observations	211,463 (9,670)	60,442 (9,125)
Redundancy	7.5 (3.3)	5.7 (5.8)
Refinement		
Resolution (Å)	33.25-1.2 (1.23-1.2)	27.99-2.4 (2.46-2.4)
n reflections	26,715 (1288)	10,043 (740)
R_{all} (%)[b]	15.03 (18.6)	19.1 (24.3)
R_{free} (%)[b]	17.58 (24.1)	23.8 (28)
n residues		
Chain A	100 (6–105)	103 (3–105)
Chain B		103 (6–105)
n ligands	1 GSH, 3 SO_4	2 GSH, 1 [2Fe-2S]
n water molecules	108	29
n atoms	978	1,662
Isotropic	122	1,662
Anisotropic	857	0
Average B-factor (Å^2)	18.5	57.6
Ramachandran statistics (%)		
Residues in preferred regions	100	97
Residues in allowed regions	0	3
Outlier residues	0	0
r.m.s.[c] deviations		
Bond length (Å)	0.025	0.021
Bond angle (°)	2.209	1.999

[a] Values in parentheses are for highest resolution shell.
[b] R_{all} was determined from all the reflections (working set + test set), whereas R_{free} corresponds to a subset of 5% of reflections (test set).
[c] Root mean square.

RESULTS

AtGrxC5, the Fourth Plastidial Grx of A. thaliana—The *A. thaliana* Grx family is composed of 33 members, which are predicted to be distributed in different subcellular compartments (11). GrxS12, -S14, and -S16 in poplar as well as GrxS14 in *A. thaliana* (previously referred to as AtGRXcp) have already been confirmed as being located in plastids by GFP fusion (20, 27, 44). From localization prediction programs, only three additional *A. thaliana* Grxs exhibit a potential plastidial targeting sequence, namely AtGrxC5 (class I), AtGrxC10, and AtGrxS13 (class III) (10, 11). It is important to note that GrxC5 and GrxS12, which form a specific subgroup of class I Grxs, display about 70% identity when considering the mature form of the proteins. The phylogenetic analysis further indicated that whereas all plants analyzed possess a GrxS12 isoform only species of the Brassicaceae family possess both isoforms (supplemental Fig. 1).

The N-terminal targeting sequences of the six putative plastidial Grxs of *A. thaliana* were fused in-frame to the green fluorescent protein variants CFP and YFP. The constructs were used to transform *A. thaliana* mesophyll protoplasts. Similarly to poplar isoforms, AtGrxS12, -S14 and -S16 are clearly located in plastids as indicated by the superimposition of the YFP or CFP signal with the chlorophyll autofluorescence in the merged images (Fig. 1). Concerning AtGrxC5, the reporter protein is also directed to the chloroplast with some dots of stronger signal within the organelle. Although the fluorescence signal for AtGrxS13 is more diffuse than for AtGrxC10, both proteins likely have a cytosolic localization at least under these experimental conditions. Therefore, these two Grxs were excluded from further analysis.

Transcript Analysis of Plastidial Grxs under Environmental Constraints—The transcript expression of AtGrxC5, -S12, -S14, and -S16 was measured using semiquantitative RT-PCR in leaves of plants grown under control and stress conditions, namely cold treatment at 4 °C, salt stress administered by watering with 150 and 300 mM NaCl solutions, and osmotic stress induced by 15% (w/v) PEG-5000 for 24 h, respectively. Under these stress conditions, the plants developed a pronounced stress phenotype (45). The signals were detected after 34 PCR cycles for GrxC5 and GrxS12, 32 cycles for GrxS14, and 30 cycles for GrxS16 (Fig. 2*A*), indicating that, in these growth conditions, GrxS16 transcripts are the most abundant within the plastidial Grx group in rosettes. Regarding environmental constraints, a significant response of the *grx* transcript level could not be observed except for a slight down-regulation under extreme salinity for AtGrxS14 and an up-regulation of AtGrxC5 in plants subjected to a cold treatment (Fig. 2*B*). Likewise only moderate

responses to diverse environmental stress conditions were found when analyzing the Affymetrix GeneChip data available via the Genevestigator tool (supplemental Table 2).

AtGrxC5 Exists in Two Forms upon Expression in E. coli—To characterize the structure-function relationship of AtGrxC5, the mature form of the protein was produced in *E. coli* as a recombinant protein by removing the N-terminal 63 residues that constitute the putative targeting sequence. The final product comprises 113 amino acids with a predicted molecular mass of 12,482 Da. As observed for PtGrxC1, lysed bacterial cells had a slight but visible brownish color (8). Similarly, following gel filtration, the protein separated into two peaks, an apoform with an apparent size corresponding to a monomer and a holoform most likely containing an Fe-S center and with an apparent exclusion volume corresponding to a dimer (supplemental Fig. 2). This result was unexpected as AtGrxC5 possesses the active site Trp residue, which was thought previously to prevent the incorporation of an Fe-S cluster in the close paralog PtGrxS12 (27).

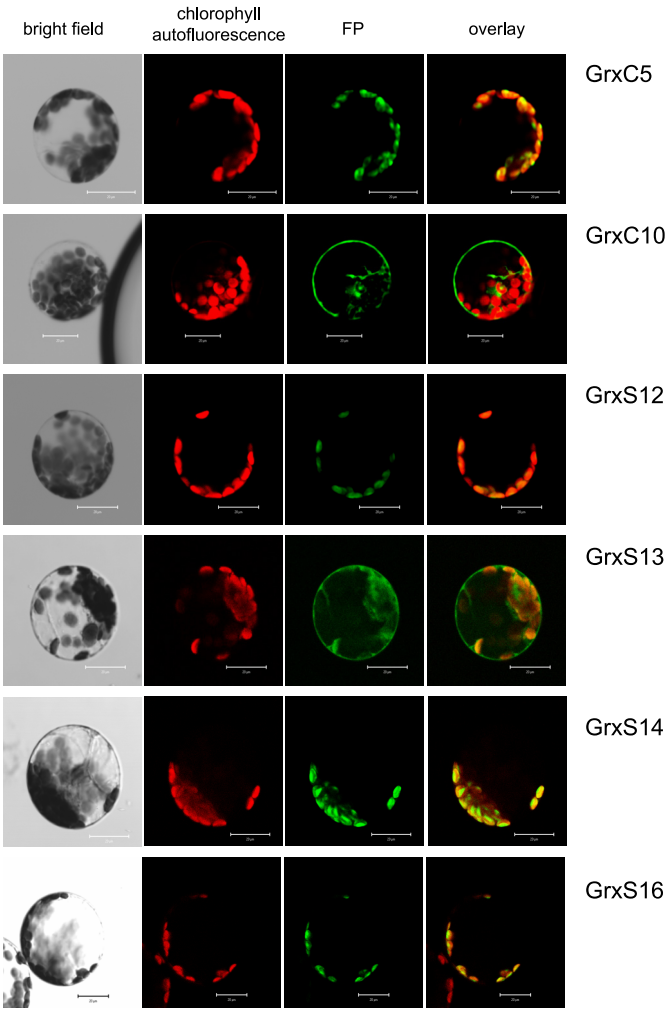

FIGURE 1. **YFP/CFP localization of putative plastidial Grxs in *A. thaliana* mesophyll protoplasts.** The sequences coding for the N-terminal extensions of AtGrxC5, AtGrxC10, AtGrxS12, AtGrxS14, AtGrxS15, and AtGrxS16 were fused in-frame with the CFP/YFP coding sequence, mesophyll protoplasts were transfected, and accumulation of the fluorescent reporter was monitored as described under "Experimental Procedures." The *scale bars* correspond to 20 μm.

The nature of the Fe-S center in holoGrxC5 was initially assessed using a combination of analytical and spectroscopic techniques. Iron and protein analyses of the holoform indicated 1.0 ± 0.2 iron/protein monomer consistent with one [2Fe-2S] cluster per dimer. This conclusion was unambiguously confirmed by the nearly identical UV-visible absorption/CD and resonance Raman spectra compared with those established for the structurally characterized PtGrxC1 (Fig. 3). Moreover, the close similarity of the spectroscopic properties of the $[2Fe\text{-}2S]^{2+}$ centers in AtGrxC5 and PtGrxC1 indicates analogous cluster coordination involving cysteinyl sulfur ligands from two GSHs and two Grxs. We have shown earlier by analyzing UV-visible absorption/CD and resonance Raman spectra that the Grx conformations are clearly distinct in class I and II Grxs, which both bind [2Fe-2S] clusters (8, 20, 26).

To determine how similar the ligation of the [2Fe-2S] cluster is to the one in PtGrxC1, the four cysteine residues of AtGrxC5 in positions 29, 32, 80, and 87 were substituted by serine residues. The substitution of either Cys^{80} or Cys^{87} did not prevent the incorporation of the Fe-S cluster. In contrast, the single substitution of Cys^{29} or Cys^{32} produced proteins that were devoid of the cluster, raising the question of the role of the second active site cysteine for cluster ligation or stability. Interestingly, a S32C variant of PtGrxS12, mimicking AtGrxC5 active site sequence, incorporated an Fe-S cluster with a UV-visible absorption spectrum similar to AtGrxC5 (supplemental Fig. 3). However, both the spectroscopic signature and the three-dimensional structure of holoGrxC5 (see below) showed that Cys^{32} is not a direct ligand for the Fe-S cluster. Next we wanted to determine whether the second cysteine is essential for cluster integration or only for its stability as observed previously for PtGrxC1. A PtGrxC1 C34S variant, although still

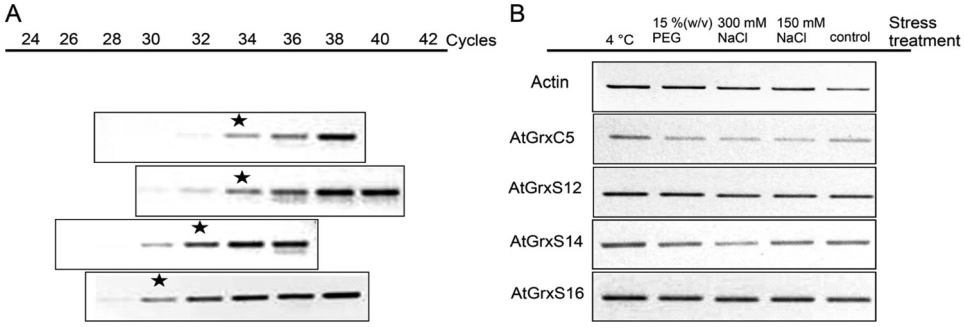

FIGURE 2. **Transcript analysis of plastidial Grxs in rosettes of *A. thaliana* wild type plants.** *A*, the abundance of Grx transcripts was semiquantified by RT-PCR. *Stars* indicate the number of cycles selected for the analysis of transcript abundance in response to the indicated stress conditions depicted in *B*. The pictures are from two independent experiments with two to three replicates with similar results.

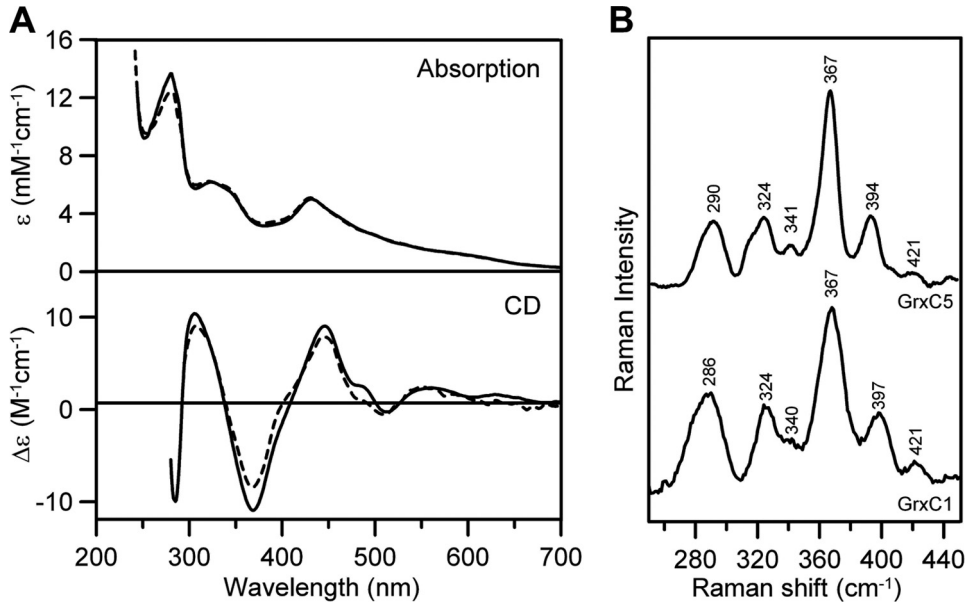

FIGURE 3. **Spectroscopic properties of AtGrxC5 holoform.** *A*, comparison of the UV-visible absorption and CD spectra of AtGrxC5 (*solid line*) and PtGrxC1 (*broken line*). ϵ and Δϵ values are expressed per Grx monomer. *B*, comparison of the resonance Raman spectra of AtGrxC5 (*solid line*) and PtGrxC1 (*broken line*) obtained at 17 K with 457.9-nm laser excitation at 7 cm^{-1} spectral bandwidth. Bands due to lattice modes of ice were subtracted from the spectra shown.

able to bind an Fe-S cluster, contained a far less stable Fe-S cluster with only 0.19 ± 0.04 iron/monomer (8). However, no Fe-S cluster could be reconstituted in AtGrxC5 C32S under anaerobic conditions following a standard procedure using glutathione and catalytic amounts of *E. coli* IscS, indicating that, in this case, the cysteine is indispensable (data not shown).

Determination of AtGrxC5 Redox State—The presence of four cysteine residues led us to investigate the redox state of the protein to better understand the catalytic mechanism utilized by the apoform of GrxC5. Whereas Cys^{29}, Cys^{32}, and Cys^{87} are conserved in many class I Grxs, Cys^{80} is not conserved even in other plant GrxC5 isoforms. Analysis by mass spectrometry of AtGrxC5 WT (purified or not in the presence of GSH) revealed the presence of three protein peaks with molecular masses of 12,348.2, 12,654.4, and 12,961.2 ± 2 Da (data not shown). Although the intensity of the different peaks varied slightly, similar results were obtained by treating prereduced AtGrxC5 with GSSG. The peak at 12,654.4 Da was generally predominant. The first peak is consistent with a protein where the methionine is cleaved. The other peaks, corresponding to mass increments of 306.2 and 613 Da, are consistent with proteins also deprived of the methionine but containing one or two glutathione adducts. After reduction with DTT, a single protein peak with a molecular mass of 12,350 Da was observed, further supporting that the protein is glutathionylated. The same three protein peaks were obtained for AtGrxC5 C80S, indicating that Cys^{80} is not a glutathionylation site. Concerning the AtGrxC5 C87S mutant, we detected two protein peaks corresponding to a reduced protein and to an oxidized protein with only one glutathione adduct, indicating that Cys^{87} is most likely one of the glutathionylation sites; the other site is either Cys^{29} or Cys^{32}. In the case of the AtGrxC5 C32S mutant, only two protein peaks corresponding to oxidized proteins with one or two glutathione adducts were detected, a result consistent with Cys^{29} and Cys^{87} being the two modified cysteines. For AtGrxC5 C29S, the protein is so unstable that we were not able to obtain reliable results confirming the loss of one glutathione adduct.

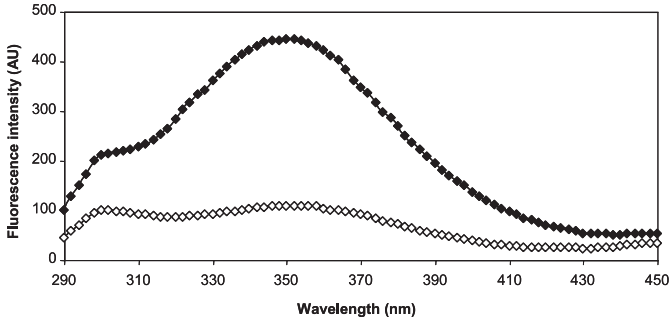

FIGURE 4. **Fluorescence spectra of AtGrxC5 under different redox states.** Emission spectra of reduced (*black squares*) and oxidized (*white squares*) apoforms of AtGrxC5 (excitation at 270 nm) were recorded with 10 μM protein at 25 °C in TE buffer. The reduced AtGrxC5 was obtained by treating the protein with 20 mM DTT before desalting on G25 columns. The prereduced AtGrxC5 was oxidized using 1 mM GSSG. *AU*, arbitrary units.

As AtGrxC5 possesses a single Trp residue as well as two Tyr residues very close to the active site at least in the primary sequence (IYSKTWCSYCT), the redox state of the apoform was also assessed by measuring its intrinsic fluorescence properties under reducing (GSH or DTT_{red}) or oxidizing (GSSG or DTT_{ox}) conditions. Reduced AtGrxC5 displayed an emission spectrum with two peaks at approximately 300 and 350 nm characteristic of a signal originating from Tyr and Trp residues, respectively (Fig. 4) (11). Addition of 1 mM GSSG but not DTT_{ox} led to the quenching of the fluorescence signal, whereas the subsequent addition of DTT_{red} restored the initial spectrum (Fig. 4 and data not shown). Because similar results were obtained for all monocysteinic mutants except AtGrxC5 C29S and because DTT_{ox} had no effect on the AtGrxC5 redox state, the fluorescence quenching can be attributed to the glutathionylation of Cys^{29}.

Reductase Activity and Catalytic Mechanism of AtGrxC5—To clarify the catalytic mechanism used by AtGrxC5 and to

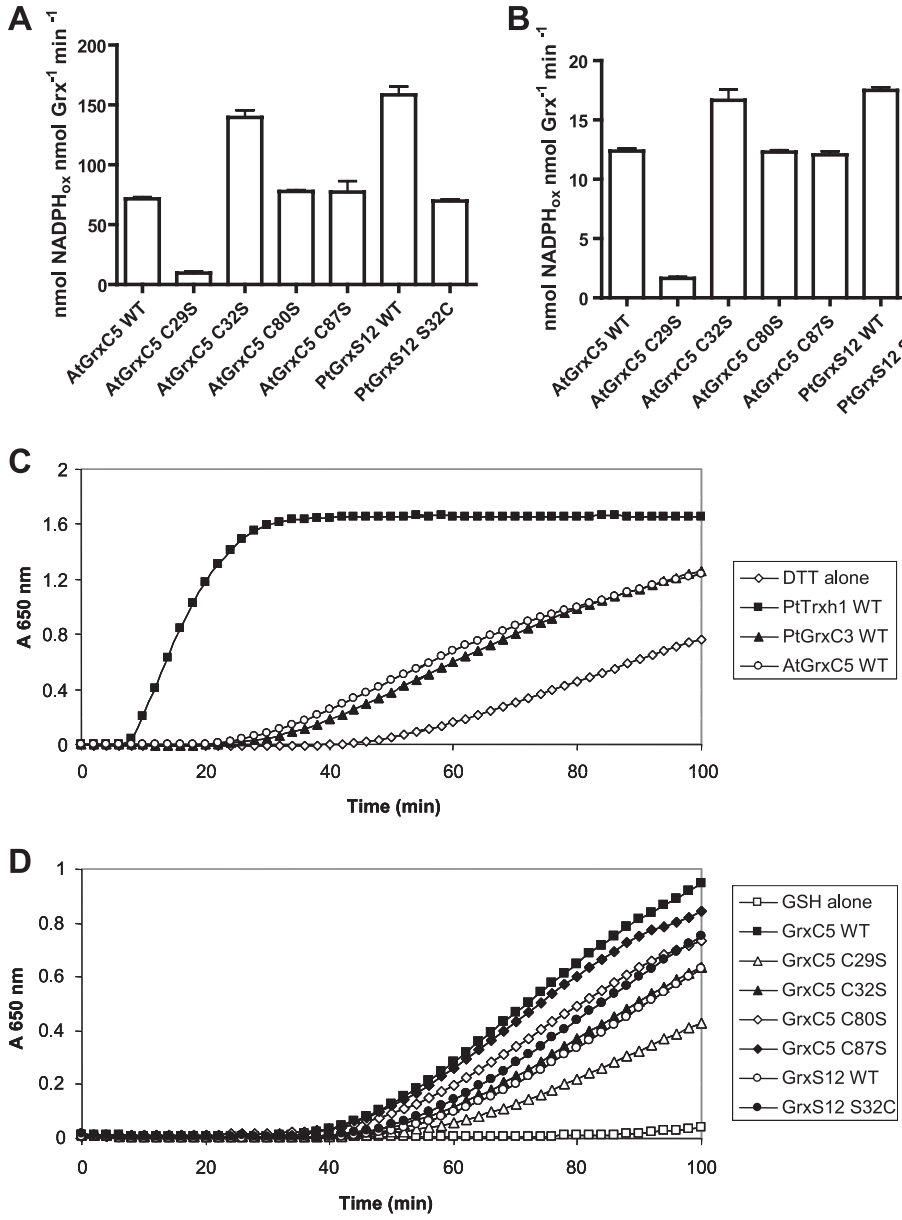

FIGURE 5. **Comparison of reductase activity between AtGrxC5 and PtGrxS12 mutants.** HED (*A*) and DHA (*B*) reduction was achieved, respectively, using 400 nM or 1 μM Grx in the presence of 2 mM GSH and either 0.7 mM HED or 1 mM DHA. The data are represented as mean ± S.D. of three separate experiments. Insulin reduction was measured either using a DTT-based assay (*C*) in the presence of 2 μM poplar Trxh1 or 10 μM Grxs or using a GSH-based assay (*D*) containing a complete GSH regeneration system (NADPH/glutathione reductase/GSH) and WT or mutated versions of AtGrxC5 and PtGrxS12.

compare its efficiency with that of PtGrxS12, we first measured the activity of all protein variants using the conventional DHA and HED assays at a fixed enzyme concentration by following NADPH oxidation in the presence of a glutathione recycling system. In both assays, we obtained very similar results: AtGrxC5 C29S was inactive, whereas AtGrxC5 C80S and AtGrxC5 C87S appeared to be as efficient as the WT protein, and AtGrxC5 C32S was nearly 2 times more efficient (Fig. 5, *A* and *B*). Strikingly, the AtGrxC5 C32S mutant, mimicking the GrxS12 active site, was as efficient as PtGrxS12, and PtGrxS12 S32C, a protein variant mimicking the GrxC5 active site, had a lower efficiency comparable with AtGrxC5 WT (Fig. 5, *A* and *B*). These results indicate that Cys^{32} is not essential for the reaction mechanism but that it influences protein reactivity.

Following these experiments, we determined the catalytic parameters of AtGrxC5 WT and all monocysteinic mutants in steady-state conditions (Table 2). During the initial preincubation time of the reaction mixture, HED and GSH give rise to a glutathionylated β-mercaptoethanol mixed disulfide (46). The kinetic analysis revealed an apparent K_m value of 0.20 ± 0.02 mM for glutathionylated β-mercaptoethanol and a k_{cat} of 1.21 ± 0.03 s^{-1}. These values are similar to those reported for human Grx2, which contains an SCSYC active site, but are lower by a factor 10–20 when compared with other class I Grxs including plant GrxC1 and -C4 (5).[5] Concerning DHA reductase activity, the results provided an apparent K_m value of 0.21 ± 0.03 mM for

[5] J. Couturier and N. Rouhier, unpublished data.

TABLE 2

Catalytic parameters for thioltransferase activity of AtGrxC5

The catalytic efficiency of AtGrxC5 WT and mutants was estimated using the HED and DHA activity assays under steady-state conditions following the procedures described under "Experimental Procedures." β-ME-SG, glutathionylated β-mercaptoethanol; ND, not determined.

Proteins	β-ME-SG			DHA			GSH		
	K_m	k_{cat}	k_{cat}/K_m	K_m	k_{cat}	k_{cat}/K_m	K_m	k_{cat}	k_{cat}/K_m
	mM	s^{-1}	M^{-1}/s^{-1}	mM	s^{-1}	M^{-1}/s^{-1}	mM	s^{-1}	M^{-1}/s^{-1}
GrxC5 WT	0.20 ± 0.02	1.21 ± 0.03	6.05×10^3	0.21 ± 0.03	0.23 ± 0.01	1.10×10^3	3.6 ± 0.8	0.69 ± 0.11	192
GrxC5 C29S	ND	ND	ND	ND	ND	ND	ND	ND	ND
GrxC5 C32S	0.31 ± 0.03	3.39 ± 0.14	1.09×10^4	0.26 ± 0.02	0.53 ± 0.02	2.04×10^4	2.4 ± 0.4	1.49 ± 0.16	621
GrxC5 C80S	0.37 ± 0.05	1.43 ± 0.07	3.86×10^3	0.18 ± 0.01	0.23 ± 0.01	1.28×10^3	3.1 ± 0.4	0.61 ± 0.05	197
GrxC5 C87S	0.58 ± 0.07	1.83 ± 0.12	3.16×10^3	0.23 ± 0.03	0.24 ± 0.01	1.04×10^3	2.6 ± 0.4	0.53 ± 0.05	204

DHA and a k_{cat} of 0.23 ± 0.01 s^{-1} (Table 2). These values are in the same order as those obtained for PtGrxS12 and CrGrx1 (6, 27). The apparent K_m value for GSH was determined by varying the amount of GSH in the DHA assay. AtGrxC5 WT possesses an apparent K_m value of 3.6 ± 0.8 mM for GSH similar to the one obtained for PtGrxS12 but also for other plant and non-plant Grxs in particular human Grx2 (5, 27). AtGrxC5 C80S and C87S possess catalytic parameters very similar to those of AtGrxC5 WT with only small variations observed in the affinity for glutathionylated β-mercaptoethanol. On the other hand, the AtGrxC5 C32S mutant displayed a better catalytic efficiency (about 2 times) compared with AtGrxC5 WT both in HED and DHA assays, originating from a better turnover number (Table 2).

In a second series of experiments, we used the classical insulin reduction assay to assess the disulfide reductase activity of AtGrxC5 (47). In the presence of DTT, AtGrxC5 and PtGrxC3, another dithiol Grx used for comparison, were able to reduce insulin but, as expected, with a lower efficiency than poplar Trxh1 (Fig. 5*C*). In alternative experiments, we measured the capacity of Grxs to reduce insulin by using an NADPH/glutathione reductase/GSH regeneration system (Fig. 5*D*). The ability of AtGrxC5 to reduce insulin was not improved compared with the DTT-based assay (Fig. 5*D*). Regarding the mutated proteins, as already observed for DHA and HED assays, AtGrxC5 C80S and AtGrxC5 C87S appeared almost as efficient as the WT protein, and AtGrxC5 C32S and PtGrxS12 S32C enzymatic activities were similar to PtGrxS12 WT and AtGrxC5 WT, respectively (Fig. 5*D*). Although delayed in time, AtGrxC5 C29S also surprisingly exhibited the capacity to slightly reduce insulin compared with the GSH alone control, possibly indicating some reactivity of the remaining cysteines toward insulin (Fig. 5*D*).

Next the capacity of AtGrxC5 to reduce putative physiological target proteins was evaluated by measuring the Grx-mediated recycling of MsrB1 and PrxIIE, two plastidial enzymes, which are efficiently reduced by GrxS12 (14, 48). Hence, as already observed for previous activity tests, AtGrxC5 C80S was as efficient as AtGrxC5 WT for the regeneration of MsrB1, whereas AtGrxC5 C32S mutant was slightly more efficient (Fig. 6*A*). On the contrary, AtGrxC5 C87S mutant was significantly less efficient as already observed for PtGrxS12 C87S mutant (Fig. 6*A*) (14). Moreover, MsrB1 possesses an apparent K_m value of 2.3 ± 0.2 μM for AtGrxC5 WT (Fig. 6*B*), a value comparable with that obtained for PtGrxS12 (14). Strictly similar results were obtained with AtPrxIIE (supplemental Fig. 4). These results are consistent with the previously described

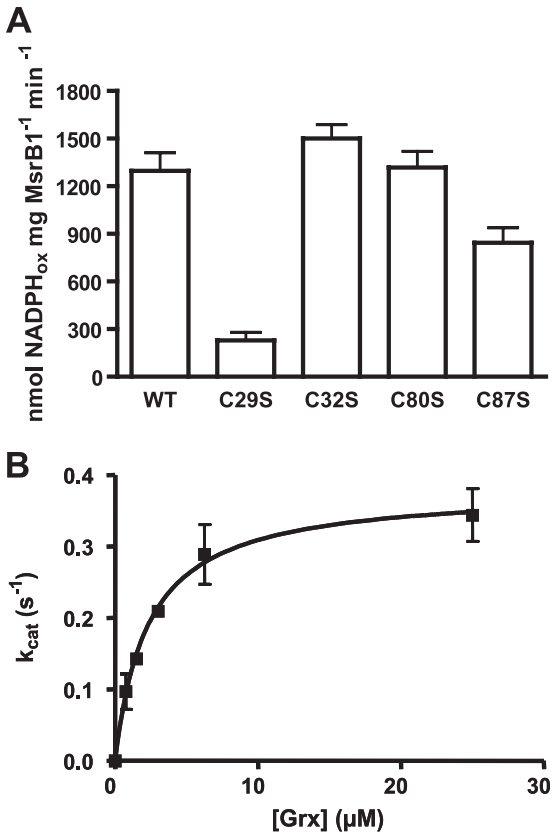

FIGURE 6. **Regeneration of AtMsrB1 by AtGrxC5 variants.** *A*, MsrB1 reduction was achieved using 25 μM GrxC5 variants. The data are represented as mean ± S.D. of three separate experiments. *B*, variation of the apparent turnover during *N*-acetylmethionine sulfoxide reduction catalyzed by 2.5 μM MsrB1 in the presence of GrxC5 WT at concentrations ranging from 0.75 to 25 μM.

regeneration mechanism of these enzymes by class I Grxs (GrxC5 or -S12) through a monothiol mechanism (14), *i.e.* (i) the reduction of the sulfenic acid by GSH followed by (ii) the deglutathionylation of the glutathione adduct by the nucleophilic attack of AtGrxC5 catalytic cysteine and (iii) the glutathione-mediated reduction of glutathionylated AtGrxC5.

Structures of GrxC5 Apo- and Holoforms and Quality of Models—The crystallographic structures of apo- ($GrxC5_{apo}$) and holoforms ($GrxC5_{holo}$) of AtGrxC5 were solved to the resolution limits of 1.2 and 2.4 Å, respectively. AtGrxC5 in the apoform crystallizes in the space group $P2_12_12$ with one glutathionylated polypeptide chain in the asymmetric unit, whereas AtGrxC5 in the holoform crystallizes in the space group *R*3, and the asymmetric unit consists of two monomers and two glutathione molecules ligating one [2Fe-2S] cluster. AtGrxC5 adopts

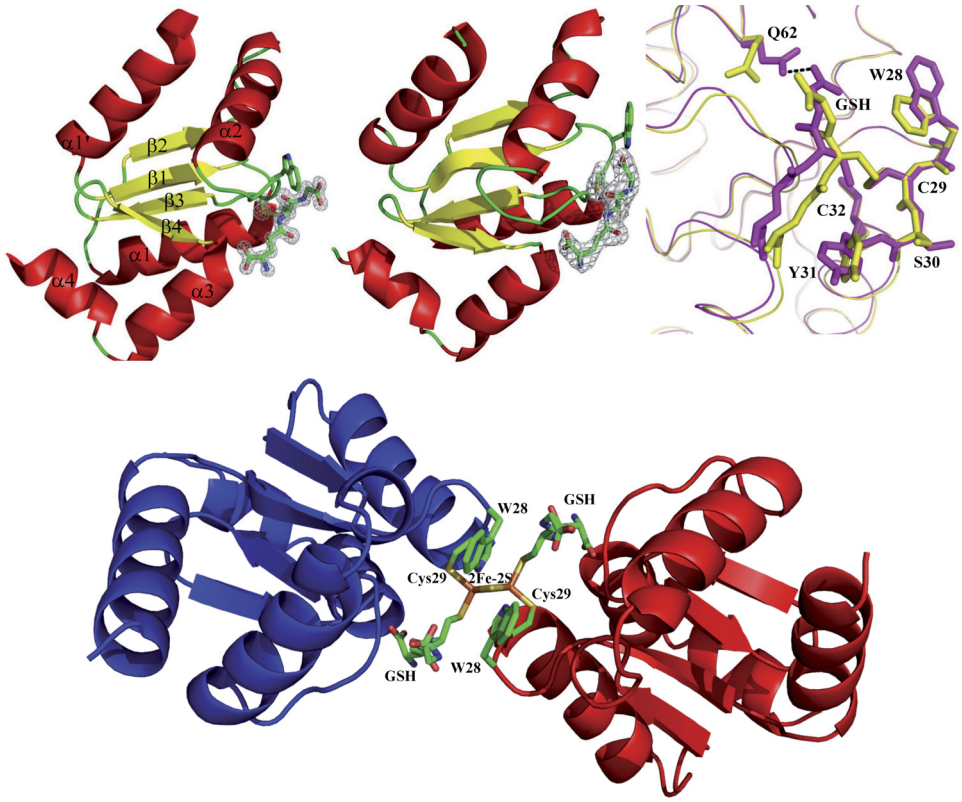

FIGURE 7. **Schematic drawing of apo- and holoform AtGrxC5 structures.** *Upper left* and *middle*, schematic representation of the overall fold of $GrxC5_{apo}$ (*left*) and $GrxC5_{holo}$ (*middle*). All α-helices are shown in *red*, β-strands are in *yellow*, and connecting loops are in *green*. Trp^{28}, Cys^{29}, and the GSH molecule are highlighted in *sticks* with final $2F_o - F_c$ electron densities (1.2σ level) covering chosen residues and ligands for clarity. Secondary structures are labeled in the *left panel*. *Upper right*, superimposition of the structures of the apoform (*yellow*) and holoform (*magenta*). The ^{28}WCSYC^{32} signature, Gln^{62}, and the GSH molecule are highlighted in *sticks*. *Bottom*, α-carbon trace of the dimer of $GrxC5_{holo}$. Monomers A and B are colored *blue* and *red*, respectively. Trp^{28}, Cys^{29}, and the GSH molecules are represented as *sticks*.

TABLE 3

Rotamers of selected side chains in AtGrxC5, poplar GrxS12, poplar GrxC1, and human Grx2 crystal structures

The dashes for the glycinyl residue indicate that no rotamer is defined because its side chain is a hydrogen atom. + represents a trans conformation, p represents a chi angle of +60°, and m a chi angle of −60°. For Trp and Tyr residues, the numeric value corresponds to chi2 angle. For Glu residue, the numeric value corresponds to chi3 angle.

AtGrxC5			PtGrxS12		PtGrxC1			hGrx2		
	apo	holo		apo		apo	holo		apo	holo
W28	p-90	p90	**W28**	p-90	**Y29**	p90	p90	**S36**	p	p
C29	t	t	**C29**	t	**C30**	t	t	**C37**	t	t
S30	p	m	**S30**	p	**G31**	-	-	**S38**	p	m
Y31	m-85	m-30	**Y31**	m-85	**Y32**	m-85	m-85	**Y39**	m-85	m-30
C32	m	m	**C32**	t	**C33**	m	m	**C40**	m	m
Q62	tp60	tt0	**Q62**	tp60	**Q62**	tt0	tt0	**Q69**	tt0	tt0

the classical Grx/Trx fold consisting of a four-stranded mixed β-sheet flanked by five α-helices (see nomenclature in Fig. 7). The crystal structures of AtGrxC5 and poplar GrxS12 are quite similar (root mean square deviation, 0.48 Å). The major difference between the two proteins concerns the presence of two additional cysteines (Cys^{32} and Cys^{80}) in AtGrxC5. The residue Cys^{80}, which is replaced by a Gly in PtGrxS12, is located in the loop between β3 and β4, and its lateral chain does not form any noticeable interaction. Cys^{32} is replaced by a serine in PtGrxS12. Both lateral chains exhibit different rotamers (Table 3). In $GrxC5_{apo}$, the thiol group of Cys^{32} is in the vicinity of the catalytic cysteine (Cys^{29}) and interacts with the backbone NH group of Lys^{26}, whereas in PtGrxS12, the side chain of Ser^{32} points toward the hydroxyl group of Ser^{25}.

In $GrxC5_{apo}$, the glutathione molecule is covalently bound to Cys^{29}, and its binding mode is identical to that of PtGrxS12 and very similar to that of other known glutathionylated Grx structures (25, 49–52). (i) The carboxylate of the glycinyl residue forms a salt bridge with the side chain of His^{72} from the loop α_2-β_3. (ii) The NH and carbonyl groups of the cysteinyl residue are hydrogen-bonded to the main chain of Val^{74}, a generally conserved residue that precedes the *cis*-Pro^{75} found in Trx superfamily members. (iii) The carboxylate of the γ-glutamate interacts with both NH groups of Cys^{87} and Thr^{88} from helix α_3. The high resolution of the electron density maps allowed us to observe two conformations for the lateral chain of Thr^{88}. Only in conformer m ($\chi_1 = -61°$) is the hydroxyl group within hydrogen bond distance from the γ-Glu carboxylate. The other possible hydrogen bond donors and acceptors of the GSH moiety interact with water molecules or symmetry-related molecules.

In the dimeric $GrxC5_{holo}$, each iron atom of the Fe-S cluster is tetracoordinated by sulfur atoms: two from the cluster, one from the catalytic Cys^{29}, and one from glutathione. A comparative structural analysis of $GrxC5_{apo}$ and $GrxC5_{holo}$ illustrates the conformational changes upon Fe-S cluster binding. All the lateral chains of the residues of the ^{28}WCYSC^{32} signature but those of the cysteines adopt different rotamers in the apo- and holoforms with Trp^{28} exhibiting flipped rotamers (Table 3). The side chain is located on the molecular surface, partially buried by a symmetry-related molecule in the apoform. Previ-

ous analyses of the PtGrxS12 crystal structure led to the conclusion that Trp^{28} cannot adopt this p-90 conformation in the dimer because of steric conflicts (27). In $GrxC5_{holo}$, the Trp^{28} rotamer observed is p90 where the NH group of the pyrrole moiety points toward the Fe-S cluster, whereas the phenyl ring is solvent-exposed (Fig. 7). The two residues Tyr^{30} and Ser^{31} also present in the signature of human (hGrx2) undergo the same conformational rearrangement upon Fe-S cluster binding in both enzymes (Table 3) (25). Gln^{62} is the last residue that attracted our attention. Indeed, in $GrxC5_{apo}$, the lateral chain participates in the stabilization of the loop α_2-β_3 containing the $^{73}TVP^{75}$ motif involved in GSH binding, whereas it adopts another rotamer in $GrxC5_{holo}$, interacting with the GSH C-terminal carboxylate group, which also undergoes a conformational change. When $GrxC5_{apo}$ and $GrxC5_{holo}$ are superposed, one noticeable difference is the backward movement of the loops α_2-β_3 and β_4-α_3, of the N-terminal part of the helix α_4, and of the glutathione molecule to accommodate the Fe-S cluster and to preserve their interactions (Fig. 7). In addition to its interaction with the carboxamide of Gln^{62}, the GSH C-terminal group is involved in a salt bridge to Lys^{36}. The rest of the new GSH/protein interactions are quaternary in nature, involving hydrogen bond donors or acceptors of the $^{28}WCSYC^{32}$ signature of monomer B for the GSH molecule of monomer A. These interactions are similar to those observed in the crystal structure of the holoform of hGrx2 (25).

DISCUSSION

GrxC5 Is the Fourth Plastidial Grx in A. thaliana—Trxs and Grxs are key players of the chloroplast redox network. Although considerable knowledge has been accumulated on chloroplastic Trx isoforms (53), the investigation of the roles of chloroplastic Grxs still lags behind. Hence, the characterization of AtGrxC5 is part of a more comprehensive work aimed at deciphering whether Grxs have specialized or redundant functions in plants and particularly in plastids.

The phylogenetic analysis of the GrxC5/S12 subgroup indicates that this subgroup is specific to land plants and that the GrxC5 isoforms are restricted to a specific plant family, the Brassicaceae, likely indicating that a single gene has been duplicated in the last common ancestor of this family. The fact that both genes have been retained suggested that they have developed specialized functions. At the transcript level, although At*GrxS12* shows slightly more expression than At*GrxC5* in rosettes, the expression of these two genes is relatively unaffected in *A. thaliana* leaves subjected to environmental constraints. Thus, despite having similar subcellular localization and transcript expression pattern, the replacement of a single amino acid in the AtGrxC5 active site cysteine conferred it specific properties.

Based on these results and on the previous characterization of GrxS12, GrxS14, and GrxS16, a model summarizing their mode of reduction and possible functions in the chloroplast has been established (Fig. 8). Importantly, GrxC5, GrxS14, and GrxS16 could exist as both apo- and holoforms, which exhibit different functionalities. From the literature on plant Grxs, it is likely that all proteins, except GrxS16, possess the capacity to deglutathionylate protein substrates, making them potential central components regulating many plastidial metabolic pathways as several glutathionylated proteins have been identified in chloroplasts (6, 54, 55). However, this reaction is likely to be preferentially carried out by class I Grxs as only GrxC5 and -S12 have the capacity to efficiently regenerate target proteins, which uses only one cysteine for catalysis, such as PrxIIE and MsrB1 (14, 48).[6] Another major difference is that the reductase activity of GrxC5 and -S12 is dependent on GSH, whereas by analogy to the work achieved with *C. reinhardtii* Grx3, GrxS14 and presumably GrxS16 may be reduced by ferredoxin-thioredoxin reductase but not glutathione (6).

Regarding the role of the holoforms, it has been suggested from experimental data or by analogy to results obtained in yeast that class II Grxs (GrxS14 and -S16), which incorporate air-labile and transferable clusters, play a role in Fe-S cluster assembly machineries or in iron sensing (56). On the contrary, AtGrxC5, which binds a more stable Fe-S cluster that cannot be transferred for example to an apoferredoxin (data not shown), should play a different role. As initially suggested for human Grx2, it could act as a redox sensor, responding to oxidative conditions (23).

Minimum Requirement for Fe-S Cluster Assembly in Grxs—The discovery that AtGrxC5 can assemble an Fe-S cluster was initially unexpected. Our results demonstrate that, among the two additional candidate cysteines present in AtGrxC5 compared with PtGrxS12, Cys^{32} determines the ability of GrxC5 to incorporate an Fe-S cluster and also influences protein activity, whereas Cys^{80} has no impact on both properties. Previous characterization of PtGrxS12 led us to conclude that the presence of a Trp residue in the active site signature prevented the incorporation of an Fe-S cluster as its replacement by a Tyr residue was sufficient to allow Fe-S center assembly (27). The present mutagenesis experiments conducted on both paralogs and their structural interpretation pointed to the importance of Cys^{32}, which is indispensable for AtGrxC5 to integrate a cluster, despite the presence of the *a priori* unfavorable Trp^{28}. Interestingly, the comparison of the crystallographic structures of PtGrxS12 and $GrxC5_{apo}$ with $GrxC5_{holo}$ showed that Trp^{28} adopts a different conformation in $GrxC5_{holo}$ with the hydrophobic part of its side chain being strikingly solvent-exposed. The beneficial effect of Cys^{32} on Fe-S cluster incorporation is likely attributed to its ability to form a hydrogen bond with the main chain of Lys^{26} ($d(S–HN) = 3.46$ Å where d is the bond distance), which would stabilize the loop containing residues 26–32 essential for Fe-S cluster binding. A serine at position 32 adopting the same conformation as Cys^{32} could not stabilize this loop because d(O–HN) would exceed 3.5 Å. This observation is consistent with the results obtained for the PtGrxC1 C34S mutant ($^{30}YCGYS^{34}$ active site) that incorporates a much more labile cluster than the WT. In this case, however, we believe that the mutant kept the ability to integrate a cluster due to the presence of Tyr^{30}, which participates in GSH stabilization.

From all these observations and the work published to date on other Fe-S-containing Grxs, it seems that, in addition to the

[6] J. Couturier and N. Rouhier, unpublished results.

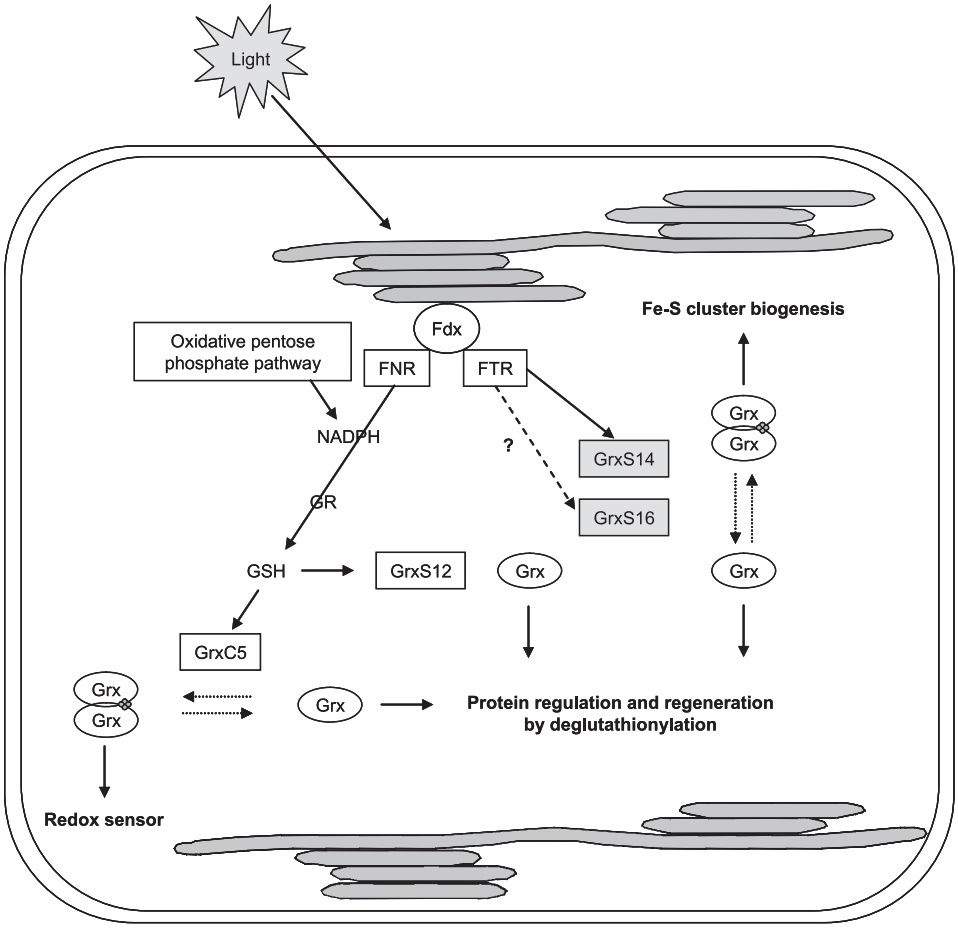

FIGURE 8. **Confirmed or potential roles for plastidial Grxs.** Grxs of class I are depicted in *white*, and those of class II are in *gray*. When the reduction pathway is not clearly demonstrated, *broken lines* are used. GrxC5, GrxS14, and GrxS16 possibly oscillate between an apomonomer and a holodimer state binding an Fe-S cluster. *Fdx*, ferredoxin; *FNR*, ferredoxin:$NADP^+$ reductase; *FTR*, ferredoxin-thioredoxin reductase; *GR*, glutathione reductase.

catalytic cysteine that is absolutely required for the [2Fe-2S] incorporation, there are at least three crucial residues at positions −1, +1, and +3 of the Cys, but they are not necessarily of the same weight (supplemental Table 3). Usually, when two residues at any of these positions have a positive effect, the protein can assemble a cluster. This is exemplified by this study where the stabilizing role of the second active site Cys in AtGrxC5, compared with PtGrxS12, could compensate for the *a priori* unfavorable effect of the Trp, which has to change its conformation without really participating in the cluster or GSH stabilization or in the dimerization.

Nevertheless, the recently identified trypanosome Grx possessing a TCPYC active site is able to incorporate an Fe-S cluster, whereas previous mutagenesis studies had suggested that the presence of the proline prevented Fe-S cluster assembly in plant and human Grxs with a YCPYC active site sequence. This indicates that an additional factor should be considered (8, 57, 58).

Role of Second Active Site Cysteines in Dithiol Grxs—Besides its importance for Fe-S cluster assembly in some Grxs, the role of the second active site Cys residue in the catalytic mechanism of dithiol Grxs remains an important open question. Its mutation affects Grx activity. However, whereas an increase in activity was observed for some yeast and mammalian dithiol Grxs (*e.g.* yeast Grx1, human Grx1 and Grx2, and pig Grx) mutated on this second active site cysteine, other studies revealed a decrease in activity as in the case of yeast Grx2 and *E. coli* Grx1 and Grx3 (5, 18, 19, 50, 52, 59–62). The difference observed between yeast Grx1 and Grx2 has been attributed, at least partially, to the nature of two residues (59). The replacement in yeast Grx2 of Ser by Ala at position 23 and of Gln by Glu at position 52 was proposed to stabilize the glutathionylated form compared with yeast Grx1. However, the absence of conservation of these two residues in other studied proteins prevents the generalization of this hypothesis.

Another recent analysis conducted with several dithiol Grxs has demonstrated that the second active site cysteine determined the glutathione specificity of the second step of peptide deglutathionylation (*i.e.* the reduction of a glutathionylated Grx by a second GSH molecule) in *E. coli* Grx1 but not in human and yeast Grx1 (61). Alternatively, the formation of an intramolecular disulfide bond between the two active site cysteines could constitute a sort of side reaction, which might serve as a protective mechanism for Grx thiol groups in some conditions, although it would certainly at the same time decrease the catalytic efficiency by slowing down Grx regeneration and thus its specific activity. However, this explanation is consistent only for yeast Grx1 and mammalian Grxs but not for yeast Grx2 and *E. coli* Grx1 and Grx3, for which, by extrapolation of the work achieved with *E. coli* Grx1, one can assume that the decrease in

activity observed is correlated to a change in glutathione recognition, binding, or affinity.

Our mutagenesis results and activity measurements clearly demonstrate that AtGrxC5 falls in the same group as mammalian Grxs and yeast Grx1, which might indicate that the second active site cysteine is not involved in the specificity of the second step of the deglutathionylation reaction either (this has yet to be experimentally confirmed) but that an intramolecular disulfide can be formed and can decrease protein reactivity. Contrary to this expectation, we were not able to find conditions allowing the formation of such an intramolecular disulfide. Instead, we found that both Cys^{29} and Cys^{87} can be stably, at least partially, glutathionylated. This is for instance very similar to PtGrxS12, a monothiol Grx, where Cys^{29} was shown to be glutathionylated and Cys^{87} was bound to a β-mercaptoethanol molecule resulting from an HED pretreatment (27). Overall, this indicates that AtGrxC5 likely functions through a monothiol mechanism involving only Cys^{29}, but it does not clarify the role of Cys^{32}.

A comparison between structures of reduced and glutathionylated forms of PtGrxC1 and human Grx2 (although GSH is not covalently linked in this case), which are both dithiol Grxs, shows that thiol groups of the active site cysteines do not adopt the same conformers in both forms (8, 24, 25). Whereas the cysteines are distant and not oriented in the same direction in the reduced forms, the thiol groups of both active site cysteines come closer upon glutathionylation, which might allow formation of an intramolecular bridge if no other unfavorable factor exists. Structural inspection of $GrxC5_{apo}$ revealed that the thiol group of Cys^{32} is present in the direct environment of Cys^{29} (Fig. 7), whereas in PtGrxS12, the side chain of Ser^{32} does not point toward Cys^{29} and would be unchanged between reduced and oxidized forms. This structural characteristic might well be responsible for the difference of a factor 2 in catalytic efficiency observed between AtGrxC5 WT or PtGrxS12 S32C, which possess a Cys, and AtGrxC5 C32S or PtGrxS12, which do not. Hence, although not forming an intramolecular disulfide, it is likely that during the catalytic cycle the proximity of Cys^{32} modifies the chemical environment of Cys^{29}, which might decrease the catalytic efficiency measured under our steady-state conditions.

Acknowledgment—Technical support from Alexandre Kriznik of the Service Commun de Biophysicochimie des Interactions Moléculaires of Nancy University is gratefully acknowledged.

REFERENCES

1. Fernandes, A. P., and Holmgren, A. (2004) *Antioxid. Redox Signal.* **6,** 63–74
2. Rouhier, N., Lemaire, S. D., and Jacquot, J. P. (2008) *Annu. Rev. Plant Biol.* **59,** 143–166
3. Martin, J. L. (1995) *Structure* **3,** 245–250
4. Fernandes, A. P., Fladvad, M., Berndt, C., Andrésen, C., Lillig, C. H., Neubauer, P., Sunnerhagen, M., Holmgren, A., and Vlamis-Gardikas, A. (2005) *J. Biol. Chem.* **280,** 24544–24552
5. Johansson, C., Lillig, C. H., and Holmgren, A. (2004) *J. Biol. Chem.* **279,** 7537–7543
6. Zaffagnini, M., Michelet, L., Massot, V., Trost, P., and Lemaire, S. D. (2008) *J. Biol. Chem.* **283,** 8868–8876
7. Aslund, F., Berndt, K. D., and Holmgren, A. (1997) *J. Biol. Chem.* **272,** 30780–30786
8. Rouhier, N., Unno, H., Bandyopadhyay, S., Masip, L., Kim, S. K., Hirasawa, M., Gualberto, J. M., Lattard, V., Kusunoki, M., Knaff, D. B., Georgiou, G., Hase, T., Johnson, M. K., and Jacquot, J. P. (2007) *Proc. Natl. Acad. Sci. U.S.A.* **104,** 7379–7384
9. Rodríguez-Manzaneque, M. T., Ros, J., Cabiscol, E., Sorribas, A., and Herrero, E. (1999) *Mol. Cell. Biol.* **19,** 8180–8190
10. Rouhier, N., Gelhaye, E., and Jacquot, J. P. (2004) *Cell. Mol. Life Sci.* **61,** 1266–1277
11. Couturier, J., Jacquot, J. P., and Rouhier, N. (2009) *Cell. Mol. Life Sci.* **66,** 2539–2557
12. Rouhier, N., Gelhaye, E., and Jacquot, J. P. (2002) *FEBS Lett.* **511,** 145–149
13. Rouhier, N., Gelhaye, E., Sautiere, P. E., Brun, A., Laurent, P., Tagu, D., Gerard, J., de Faÿ, E., Meyer, Y., and Jacquot, J. P. (2001) *Plant Physiol.* **127,** 1299–1309
14. Tarrago, L., Laugier, E., Zaffagnini, M., Marchand, C., Le Maréchal, P., Rouhier, N., Lemaire, S. D., and Rey, P. (2009) *J. Biol. Chem.* **284,** 18963–18971
15. Vieira Dos Santos, C., Laugier, E., Tarrago, L., Massot, V., Issakidis-Bourguet, E., Rouhier, N., and Rey, P. (2007) *FEBS Lett.* **581,** 4371–4376
16. Greetham, D., Vickerstaff, J., Shenton, D., Perrone, G. G., Dawes, I. W., and Grant, C. M. (2010) *BMC Biochem.* **11,** 3
17. Dalle-Donne, I., Rossi, R., Colombo, G., Giustarini, D., and Milzani, A. (2009) *Trends Biochem. Sci.* **34,** 85–96
18. Bushweller, J. H., Aslund, F., Wüthrich, K., and Holmgren, A. (1992) *Biochemistry* **31,** 9288–9293
19. Peltoniemi, M. J., Karala, A. R., Jurvansuu, J. K., Kinnula, V. L., and Ruddock, L. W. (2006) *J. Biol. Chem.* **281,** 33107–33114
20. Bandyopadhyay, S., Gama, F., Molina-Navarro, M. M., Gualberto, J. M., Claxton, R., Naik, S. G., Huynh, B. H., Herrero, E., Jacquot, J. P., Johnson, M. K., and Rouhier, N. (2008) *EMBO J.* **27,** 1122–1133
21. Molina-Navarro, M. M., Casas, C., Piedrafita, L., Bellí, G., and Herrero, E. (2006) *FEBS Lett.* **580,** 2273–2280
22. Rodríguez-Manzaneque, M. T., Tamarit, J., Bellí, G., Ros, J., and Herrero, E. (2002) *Mol. Biol. Cell* **13,** 1109–1121
23. Lillig, C. H., Berndt, C., Vergnolle, O., Lönn, M. E., Hudemann, C., Bill, E., and Holmgren, A. (2005) *Proc. Natl. Acad. Sci. U.S.A.* **102,** 8168–8173
24. Feng, Y., Zhong, N., Rouhier, N., Hase, T., Kusunoki, M., Jacquot, J. P., Jin, C., and Xia, B. (2006) *Biochemistry* **45,** 7998–8008
25. Johansson, C., Kavanagh, K. L., Gileadi, O., and Oppermann, U. (2007) *J. Biol. Chem.* **282,** 3077–3082
26. Iwema, T., Picciocchi, A., Traore, D. A., Ferrer, J. L., Chauvat, F., and Jacquamet, L. (2009) *Biochemistry* **48,** 6041–6043
27. Couturier, J., Koh, C. S., Zaffagnini, M., Winger, A. M., Gualberto, J. M., Corbier, C., Decottignies, P., Jacquot, J. P., Lemaire, S. D., Didierjean, C., and Rouhier, N. (2009) *J. Biol. Chem.* **284,** 9299–9310
28. Schenk, P. M., Baumann, S., Mattes, R., and Steinbiss, H. H. (1995) *BioTechniques* **19,** 196–198, 200
29. Couturier, J., Didierjean, C., Jacquot, J. P., and Rouhier, N. (2010) *Biochem. Biophys. Res. Commun.* **403,** 435–441
30. Behm, M., and Jacquot, J. P. (2000) *Plant Physiol. Biochem.* **38,** 363–369
31. Horling, F., Lamkemeyer, P., König, J., Finkemeier, I., Kandlbinder, A., Baier, M., and Dietz, K. J. (2003) *Plant Physiol.* **131,** 317–325
32. Wormuth, D., Baier, M., Kandlbinder, A., Scheibe, R., Hartung, W., and Dietz, K. J. (2006) *BMC Plant Biol.* **6,** 15
33. Seidel, T., Golldack, D., and Dietz, K. J. (2005) *FEBS Lett.* **579,** 4374–4382
34. Brown, R. E., Jarvis, K. L., and Hyland, K. J. (1989) *Anal. Biochem.* **180,** 136–139
35. Fish, W. W. (1988) *Methods Enzymol.* **158,** 357–364
36. Crouse, B. R., Sellers, V. M., Finnegan, M. G., Dailey, H. A., and Johnson, M. K. (1996) *Biochemistry* **35,** 16222–16229
37. Kabsch, W. (1993) *J. Appl. Crystallogr.* **26,** 795–800
38. CCP4: Collaborative Computational Project. Number 4 (1994) *Acta Crystallogr. D Biol. Crystallogr.* **50,** 760–763
39. Evans, P. (2006) *Acta Crystallogr. D Biol. Crystallogr.* **62,** 72–82
40. Vagin, A., and Teplyakov, A. (1997) *J. Appl. Crystallogr.* **30,** 1022–1025

41. Murshudov, G. N., Vagin, A. A., and Dodson, E. J. (1997) *Acta Crystallogr. D Biol. Crystallogr.* **53,** 240–255
42. Emsley, P., Lohkamp, B., Scott, W. G., and Cowtan, K. (2010) *Acta Crystallogr. D Biol. Crystallogr.* **66,** 486–501
43. Chen, V. B., Arendall, W. B., 3rd, Headd, J. J., Keedy, D. A., Immormino, R. M., Kapral, G. J., Murray, L. W., Richardson, J. S., and Richardson, D. C. (2010) *Acta Crystallogr. D Biol. Crystallogr.* **66,** 12–21
44. Cheng, N. H., Liu, J. Z., Brock, A., Nelson, R. S., and Hirschi, K. D. (2006) *J. Biol. Chem.* **281,** 26280–26288
45. Ströher, E., Wang, X. J., Roloff, N., Klein, P., Husemann, A., and Dietz, K. J. (2009) *Mol. Plant* **2,** 357–367
46. Luthman, M., and Holmgren, A. (1982) *J. Biol. Chem.* **257,** 6686–6690
47. Holmgren, A. (1979) *J. Biol. Chem.* **254,** 9627–9632
48. Gama, F., Bréhélin, C., Gelhaye, E., Meyer, Y., Jacquot, J. P., Rey, P., and Rouhier, N. (2008) *Physiol. Plant* **133,** 599–610
49. Nikkola, M., Gleason, F. K., Saarinen, M., Joelson, T., Björnberg, O., and Eklund, H. (1991) *J. Biol. Chem.* **266,** 16105–16112
50. Nordstrand, K., slund, F., Holmgren, A., Otting, G., and Berndt, K. D. (1999) *J. Mol. Biol.* **286,** 541–552
51. Xia, T. H., Bushweller, J. H., Sodano, P., Billeter, M., Björnberg, O., Holmgren, A., and Wüthrich, K. (1992) *Protein Sci.* **1,** 310–321
52. Yang, Y., Jao, S., Nanduri, S., Starke, D. W., Mieyal, J. J., and Qin, J. (1998) *Biochemistry* **37,** 17145–17156
53. Meyer, Y., Siala, W., Bashandy, T., Riondet, C., Vignols, F., and Reichheld, J. P. (2008) *Biochim. Biophys. Acta* **1783,** 589–600
54. Gao, X. H., Zaffagnini, M., Bedhomme, M., Michelet, L., Cassier-Chauvat, C., Decottignies, P., and Lemaire, S. D. (2010) *FEBS Lett.* **584,** 2242–2248
55. Michelet, L., Zaffagnini, M., Vanacker, H., Le Maréchal, P., Marchand, C., Schroda, M., Lemaire, S. D., and Decottignies, P. (2008) *J. Biol. Chem.* **283,** 21571–21578
56. Rouhier, N., Couturier, J., Johnson, M. K., and Jacquot, J. P. (2010) *Trends Biochem. Sci.* **35,** 43–52
57. Berndt, C., Hudemann, C., Hanschmann, E. M., Axelsson, R., Holmgren, A., and Lillig, C. H. (2007) *Antioxid. Redox Signal.* **9,** 151–157
58. Ceylan, S., Seidel, V., Ziebart, N., Berndt, C., Dirdjaja, N., and Krauth-Siegel, R. L. (2010) *J. Biol. Chem.* **285,** 35224–35237
59. Discola, K. F., de Oliveira, M. A., Rosa Cussiol, J. R., Monteiro, G., Bárcena, J. A., Porras, P., Padilla, C. A., Guimarães, B. G., and Netto, L. E. (2009) *J. Mol. Biol.* **385,** 889–901
60. Gallogly, M. M., Starke, D. W., Leonberg, A. K., Ospina, S. M., and Mieyal, J. J. (2008) *Biochemistry* **47,** 11144–11157
61. Saaranen, M. J., Salo, K. E., Latva-Ranta, M. K., Kinnula, V. L., and Ruddock, L. W. (2009) *Antioxid. Redox Signal.* **11,** 1819–1828
62. Yang, Y. F., and Wells, W. W. (1991) *J. Biol. Chem.* **266,** 12759–12765